

Article

Research on Drought Monitoring Based on Deep Learning: A Case Study of the Huang-Huai-Hai Region in China

Junwei Zhou, Yanguo Fan, Qingchun Guan *  and Guangyue Feng

College of Oceanography and Space Informatics, China University of Petroleum (East China), Qingdao 266580, China; s21160029@s.upc.edu.cn (J.Z.); ygf@upc.edu.cn (Y.F.); z21160108@s.upc.edu.cn (G.F.)
* Correspondence: qingchunguan@upc.edu.cn

Abstract: As climate change intensifies, drought has become a major global engineering and environmental challenge. In critical areas such as agricultural production, accurate drought monitoring is vital for the sustainable development of regional agriculture. Currently, despite extensive use of traditional meteorological stations and remote sensing methods, these approaches have proven to be inadequate in capturing the full extent of drought information and adequately reflecting spatial characteristics. Therefore, to improve the accuracy of drought forecasts and achieve predictions across extensive areas, this paper employs deep learning models, specifically introducing an attention-weighted long short-term memory network model (AW-LSTM), constructs a composite drought monitoring index (CDMI) and validates the model. Results show that: (1) The AW-LSTM model significantly outperforms traditional long short-term memory (LSTM), support vector machine (SVM) and artificial neural network (ANN) models in drought monitoring, offering not only better applicability in meteorological and agricultural drought monitoring but also the ability to accurately predict drought events one month in advance compared to machine learning models, providing a new method for precise and comprehensive regional drought assessment. (2) The Huang-Huai-Hai Plain has shown significant regional variations in drought conditions across different years and months, with the drought situation gradually worsening in the northern part of Hebei Province, Beijing, Tianjin, the southern part of Huai North and the central part of Henan Province from 2001 to 2022, while drought conditions in the northern part of Huai North, southern Shandong Province, western Henan Province and southwestern Hebei Province have been alleviated. (3) During the sowing (June) and harvesting (September) periods for summer maize, the likelihood of drought occurrences is higher, necessitating flexible adjustments to agricultural production strategies to adapt to varying drought conditions.

Keywords: deep learning; long short-term memory networks; drought monitoring; Huang-Huai-Hai Plain



Citation: Zhou, J.; Fan, Y.; Guan, Q.; Feng, G. Research on Drought Monitoring Based on Deep Learning: A Case Study of the Huang-Huai-Hai Region in China. *Land* **2024**, *13*, 615. <https://doi.org/10.3390/land13050615>

Academic Editor: Hariklia D. Skilodimou

Received: 8 March 2024

Revised: 23 April 2024

Accepted: 30 April 2024

Published: 2 May 2024



Copyright: © 2024 by the authors. Licensee MDPI, Basel, Switzerland. This article is an open access article distributed under the terms and conditions of the Creative Commons Attribution (CC BY) license (<https://creativecommons.org/licenses/by/4.0/>).

1. Introduction

Drought, as an extreme climatic event, poses a serious challenge to global food security [1,2]. As global warming intensifies, water scarcity is becoming more acute, leading to an increase in the intensity, frequency and duration of droughts, making drought trends a global concern [3]. China, a major agricultural country, suffers significant losses in agricultural production and national economic development due to frequent droughts caused by the instability of annual monsoons and the complexity of natural geographical features, resulting in uneven distribution of water and heat [4,5]. According to statistics, since the 21st century, food losses have doubled compared to the 1980s, with an annual average food loss due to drought of 37.284 million tons [6]. In 2022, droughts in China affected an area of 6.09 million hectares of crops, accounting for 50.45% of the total area affected by natural disasters that year; food losses amounted to 5.744 million tons, economic crop losses reached CNY 14.944 billion and the direct economic losses were up to CNY 51.285 billion [7]. This

shows that drought has a severe impact on agricultural production in China, posing a serious threat to China's food security and sustainable development. Therefore, understanding the changes and trends in agricultural drought problems, improving the effective monitoring and accurate prediction of drought and minimising the economic and social losses caused by drought are of great importance to national and social stability.

Current drought monitoring methods include traditional meteorological monitoring and remote sensing [8–10]. Meteorological monitoring offers high accuracy and ease of data acquisition but lacks spatial continuity and cannot precisely monitor the spatial distribution of drought conditions; remote sensing can collect surface parameters in real-time over large areas, helping to comprehensively reflect the moisture conditions of soil and vegetation and reveal actual imbalances in water balance, but it is often limited to single or few indicators, overlooking the multifactorial complexity of droughts. To overcome these limitations, many scholars have recently endeavoured to combine various factors influencing drought to construct comprehensive monitoring models [11–14]. For example, Wang and others [15] in the North China Plain integrated seven drought indices to create the Aggregate Drought Index (ADI), which was then used to quantitatively analyse the impact of drought on crop yields, especially examining the relationship between climate yield variability of winter wheat and ADI values through time series and panel regression models. Similarly, Yu Haozhe and colleagues [16] combined indices such as the Precipitation Condition Index (PCI), Vegetation Condition Index (VCI) and Temperature Condition Index (TCI) through a multivariate linear regression model to create the Comprehensive Drought Index (CDI), which allows for more accurate monitoring of drought conditions in the Jing-Jin-Ji region. In another study, Xu and others [17] utilized the Copula function and data on precipitation, potential evapotranspiration and soil moisture to develop the Standard Precipitation, Potential Evapotranspiration and Root-Zone Soil Moisture Index (SPESMI) for Henan Province, highlighting its applicability in agricultural drought monitoring and its ability to capture seasonal variations. Furthermore, ArunKumar and colleagues [18] integrated indices such as the Precipitation Condition Index (PCI), Temperature Condition Index (TCI), Soil Moisture Condition Index (SMCI) and Vegetation Condition Index (VCI), applying principal component analysis to develop the Integrated Drought Monitoring Index (IDMI), effectively used for assessing and monitoring agricultural drought in southeastern India.

Although current drought monitoring research has made some progress, there are still significant shortcomings: traditional regression methods rely on multiple experiments to determine weights and assume that drought-causing factors are limited, which restricts their ability to handle complex environments; moreover, although traditional machine learning methods can process multidimensional data, they require tedious feature selection and dimension reduction in practical applications [19,20]. In contrast, deep learning can automatically learn and extract data features through a layered neural network structure, thus avoiding manual intervention and improving prediction accuracy. In building comprehensive drought monitoring models, deep learning algorithms can extract more useful features from a multitude of drought factors [21,22]. For example, Dikshit and others have demonstrated that using recurrent neural networks (RNNs) and long short-term memory networks (LSTMs) can effectively predict drought [23]. However, most current research applying deep learning to drought monitoring remains limited to basic model stages. Most existing studies focus on implementing and testing standard neural network models, such as basic RNNs and LSTMs, without delving into or customizing more complex network structures and algorithm optimizations to meet the specific needs and challenges of drought prediction. Therefore, this study enhances the LSTM model by further optimizing it and introducing an attention mechanism to improve the model's efficiency in recognizing key features over long time sequences, aiming to significantly increase the accuracy and practicality of drought predictions.

2. Materials and Methods

2.1. Study Area

The Huang-Huai-Hai Plain is one of the three major plains of China and is the most populous. The plain is located between 32~40° N and 114~121° E [24]. A map of the study area is shown in Figure 1. This region has a temperate monsoon climate, with hot and humid summers, cold and dry winters and distinct seasons. Average annual rainfall is 480–1050 mm [25], unevenly distributed across the region, with less in the north and more in the south. The terrain is mainly plain, but includes some low mountainous and hilly areas, with an overall flat topography and low elevations. The region is traversed by rivers such as the Yellow, Huai and Hai Rivers, which form a rich network of water systems across the plains and play a crucial role in local irrigation and agricultural development [26]. The total arable land area of the Huang-Huai-Hai Plain is 214,000 square kilometres, of which 40.15% is first- to third-class arable land, 49.22% is fourth- to sixth-class arable land and 10.64% is seventh to tenth class arable land [27]. Corn is grown on an area of 60,000 square kilometres, with a total production of around 2.2 billion tonnes, mainly planted between June and September [28]. The excellent geographical conditions of the region greatly enhance agricultural production.

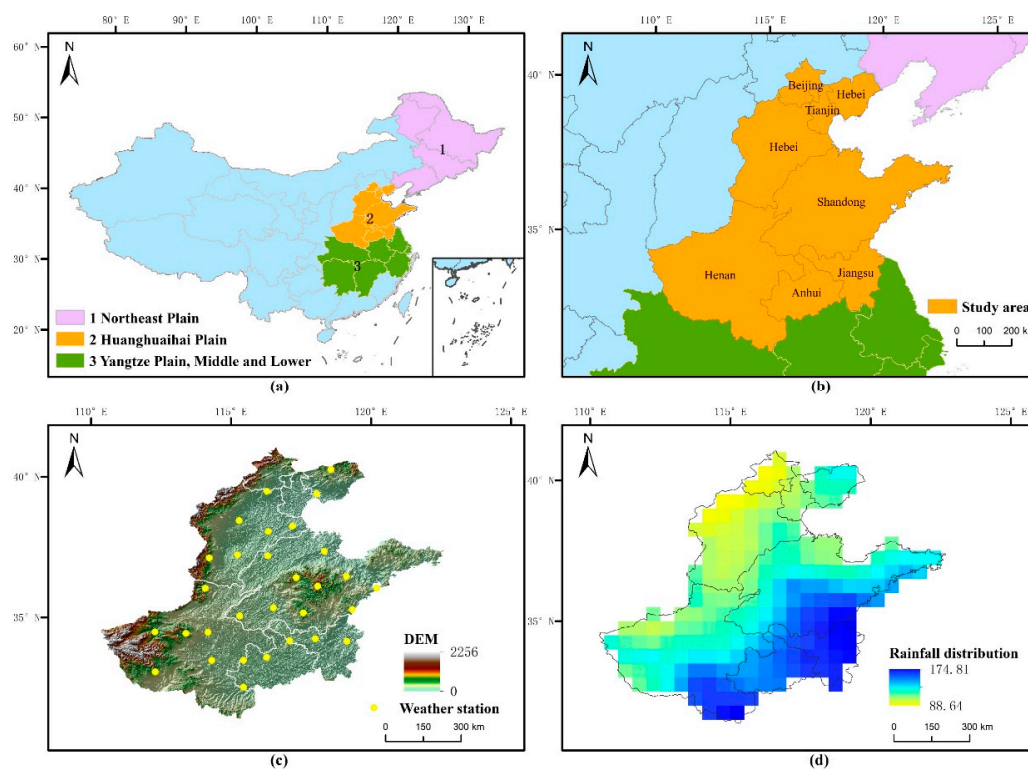


Figure 1. Overview of the study area. (a) Geographic location of the study area. (b) Administrative division map of the study area. (c) Elevation map and distribution of meteorological stations in the study area. (d) Rainfall distribution in the study area.

2.2. Data Preparation and Processing

2.2.1. CRU_TS Data

This study uses the CRU_TS (Climatic Research Unit Gridded Time Series) data produced by the Climate Research Unit of the University of East Anglia in Norwich, England. This dataset has a resolution of 0.5°, covers all land areas of the globe except Antarctica, spans 1901 to 2022 and includes ten observed and derived variables, with some missing values within regions. The CRU_TS dataset has been widely used for drought monitoring and has undergone comprehensive review and validation [29,30]. The dataset can be downloaded from the East Anglia University Climate Research Unit website

(<https://catalogue.ceda.ac.uk>), accessed on 14 April 2024. This research selected seven variables from the dataset, categorized into primary variables (precipitation and average temperature), secondary variables (vapor pressure and cloud cover) and derived variables (minimum temperature, maximum temperature and potential evapotranspiration). Additionally, this study utilized the global SPEI (Standardized Precipitation Evapotranspiration Index) database from the CRU dataset, downloading global SPEI data on a three-month timescale, available at <https://spei.csic.es/database.html>, accessed on 14 April 2024.

2.2.2. Land Use Data

The land use data utilized in this study come from two significant databases. The land use data from 1980 to 2015 were provided by the National Tibetan Plateau Data Centre (<https://data.tpdc.ac.cn>, accessed on 14 April 2024) issued every five years, totalling seven periods, with a spatial resolution of 1 km. The global land use classification maps from 2017 to 2021 were supplied by the Environmental Systems Research Institute (ESRI), available at (<https://livingatlas.arcgis.com>, accessed on 14 April 2024) with data released annually and a spatial resolution of 10 m. In this study, covering the period from 2001 to 2022, land use classification maps from 2000 and 2021 were specifically selected as key time points for analysis. The 2000 data serves as the starting point for the study period and the 2021 data represents the most recent land use data in the dataset. The analysis of land use differences between these two times discusses the potential impacts these differences might have on drought trend analysis. Land use classification maps for 2000 and 2021 are shown in Figure 2.

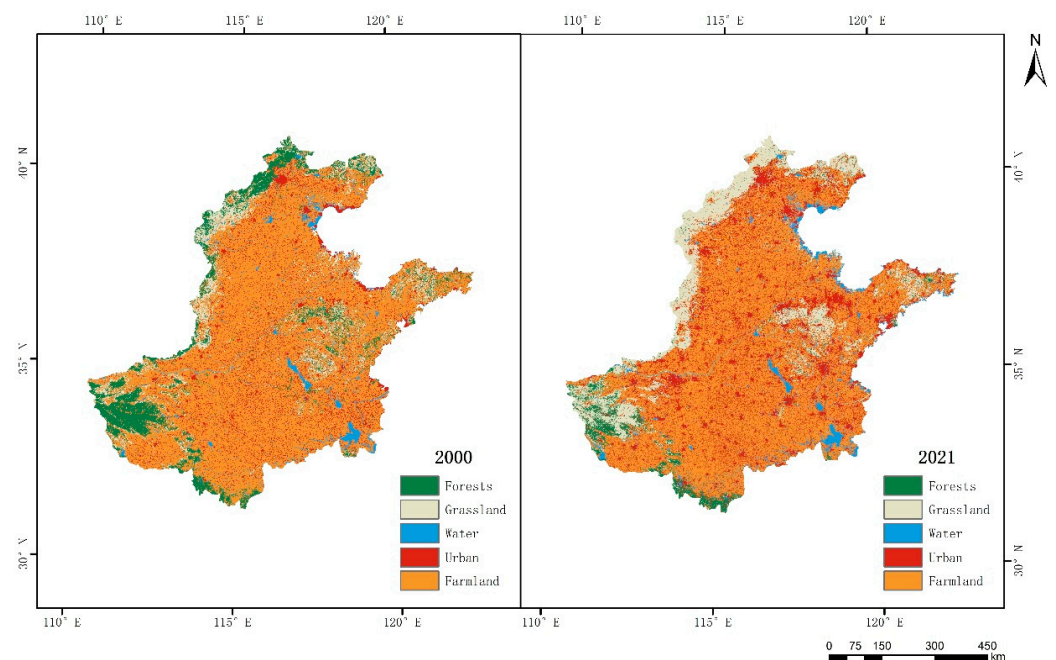


Figure 2. Land use classification for 2000 and 2021.

2.2.3. Meteorological Data

The meteorological data used in this study include monthly precipitation, average monthly temperature and 10 cm soil moisture data, covering 30 weather stations across the Huang-Huai-Hai Plain, from January 2001 to December 2022. Detailed information on the meteorological observation stations involved in the study can be found in Table 1. The data were sourced from the China Meteorological Data Network (<http://data.cma.cn/>, accessed on 14 April 2024).

Table 1. Information on meteorological observation stations in the study.

Area Station Name	Longitude	Latitude	Area Station Name	Longitude	Latitude
Bozhou	115.44	33.47	Nanyang	112.29	33.06
Fuyang	115.44	32.52	Xihua	114.31	33.47
Beijing	116.28	39.48	Yongcheng	116.27	33.58
Xingtai	114.22	37.11	Pizhou	118.01	34.24
Qinglong	118.57	40.25	Xuzhou	117.09	34.17
Tangshan	118.06	39.39	Guanyun	119.14	34.15
Baoding	115.29	38.44	Lingcheng	116.31	37.19
Botou	116.33	38.05	Zhangqiu	117.33	36.41
Huanghua	117.19	38.24	Kenli	118.33	37.35
Nangong	115.23	37.22	Yiyuan	118.1	36.11
Anyang	114.08	36.03	Weifang	119.12	36.45
Mengjin	112.28	34.48	Qingdao	120.2	36.04
Zhengzhou	113.39	34.43	Dingtao	115.31	35.05
Kaifeng	114.18	34.47	Yanzhou	116.51	35.34

2.2.4. Other Data

Other data include summer maize yield data, agricultural water usage data, population data and GDP data. Statistics from 2006 to 2021 for the five provinces of the Huang-Huai-Hai Plain (Shandong, Hebei, Henan, Beijing, Tianjin) on summer maize planted area yield, population, GDP and agricultural water usage are all sourced from the China Statistical Yearbook (<https://www.stats.gov.cn>, accessed on 14 April 2024).

2.2.5. Data Preprocessing

(1) CRU_TS Data Processing

Verify the time and spatial match of the data, check for missing and outlier values and confirm the consistency of measurements and units across all data sources. Convert NETCDF4 data format uniformly to TIF format and define the WGS84 coordinate system for the data. Background values are set to an extreme value and ignored during processing. Check the shape of input data to ensure all data have the same shape for reshaping. In machine learning and deep learning, input values of different proportions need to be normalized. Normalization ensures that observations follow a Gaussian distribution, using their mean and standard deviation rather than extreme values to ensure the robustness of new data. This study uses sklearn's StandardScaler to normalize the dataset, ensuring consistent interpretation and evaluation standards for all features.

(2) Land Use Data Processing

This study standardized the land use data for 2000 and 2021 to the WGS-84 coordinate system and resampled the spatial resolution of 2021 data to 1 km to match the resolution of 2000 data. Land cover types were categorized into five classes: forests, grassland, water, urban and farmland.

2.3. Modelling of Attention-Weighted Long- and Short-Term Memory Networks

Machine learning models analyse and train large datasets of disaster-causing factors to reveal the interrelationships among these factors. RNNs consider both current and previous input data to map target vectors, offering significant advantages over traditional neural network models that rely solely on weight multiplication. Additionally, RNNs can store internal memories of previous inputs, allowing them to reflect on past events, which is crucial in fields like drought prediction [21]. However, RNNs may face issues of vanishing and exploding gradients when stacked, a problem effectively addressed by the introduction of long short-term memory networks (LSTMs) [31]. LSTMs were proposed by Hochreiter and Schmidhuber in 1997 [32] and have been extensively developed and applied in subsequent research.

Recurrent neural networks utilize a chain of repeated neural network modules. For example, in a standard RNN, this repeating module structure is very simple, containing only a tanh layer. LSTMs also adopt a chain-like structure, but their repeating module is constructed differently, consisting of four interacting layers instead of a single neural network layer. In LSTMs, the core components are gate structures that control the flow of information. These include the forget gate (deciding which information to discard), the input gate (selecting information to update the memory state) and the output gate (determining the output based on the input and memory state). The forget and input gates are responsible for updating the internal state, while the output gate controls the final output. The functioning of the gates and the information flow can be represented by specific mathematical equations [33,34]. The formulas are as follows:

$$f_t = \sigma(W_f[h_{t-1}, x_t] + b_f) \quad (1)$$

$$i_t = \sigma(W_i[h_{t-1}, x_t] + b_i) \quad (2)$$

$$\tilde{C}_t = \tanh(W_C[h_{t-1}, x_t] + b_C) \quad (3)$$

$$C_t = f_t \times C_{t-1} + i_t \times \tilde{C}_t \quad (4)$$

$$o_t = \sigma(W_o[h_{t-1}, x_t] + b_o) \quad (5)$$

$$h_t = o_t \times \tanh(C_t) \quad (6)$$

where x_t is the input vector at time t , σ is the activation function such as sigmoid, Relu function. W_f , W_i , W_C and W_o are the weights of the new input x_t and the output h_{t-1} from the previous unit, where b_f , b_i , b_C and b_o are the corresponding biases. f_t , i_t and o_t are the outputs of the three sigmoid σ functions and have values in the range 0–1.

This study proposes a new network model—attention-weighted long short-term memory (AW-LSTM)—by integrating an attention mechanism into the long short-term memory network (LSTM) to enhance the model's performance and improve its ability to recognize long-distance dependencies. The model structure is shown in Figure 3. The model consists of two parts:

- (1) The first part is the channel attention mechanism, which emphasizes key features and weakens others by assigning weights to the feature sequence. The weight coefficients are calculated through two fully connected layers after average pooling. The first fully connected layer uses a RELU activation function and the second uses a Sigmoid activation function. Initially, the average pooling layer reduces the dimensions and captures global features; then, two fully connected layers process the pooled data, where the first layer reduces dimensions and the second restores them, outputting attention scores for each channel.
- (2) The second part is the LSTM layer, a recurrent neural network layer for processing time series. In the model, the channel attention mechanism first weights the input data, which is then fed into a two-layer LSTM structure. The first layer has a hidden dimension of 50, utilizing the LSTM's temporal processing capabilities to extract features from sequence data. The second layer, with a hidden dimension of 25, helps capture more complex temporal dependencies and enhances model performance. Finally, after passing through a fully connected layer, the output layer produces the predicted values. Repeated experiments have shown that this structural design achieves optimal predictive performance.

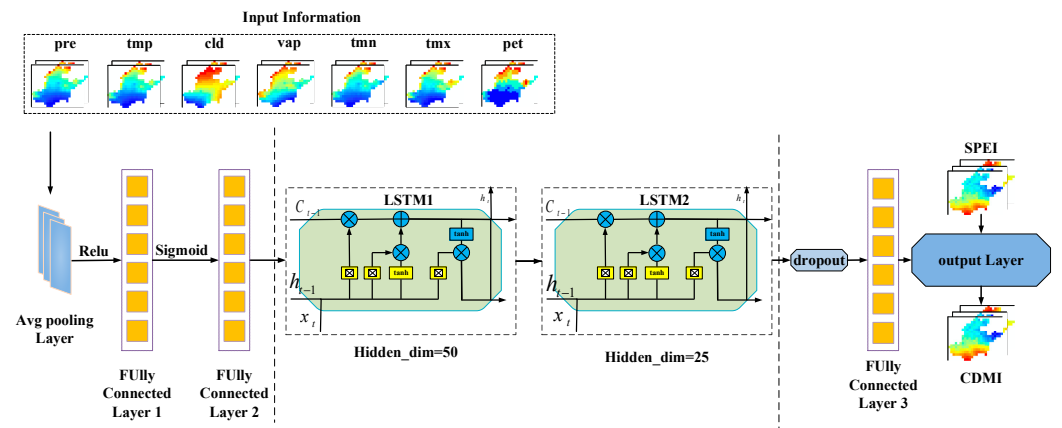


Figure 3. Structure of the AW-LSTM mode.

Regarding dataset division, data from 1901 to 2000 is used for training, while data from 2001 to 2022 is used for validation. The input to the network is in the form of a 3D tensor, represented as [sample_size, time_steps, features]. Here, sample_size is the training data, monthly data from 1901 to 2000. time_steps is the size of the time window used for predicting CDMI, set to 3, meaning the parameters from the previous three months are used to predict the Composite Drought Monitoring Index (CDMI) for the fourth month. features represents the number of weather variables used to predict CDMI; in this study, 7 variables are used, thus the value is 7. In the model, a dropout mechanism is added to prevent overfitting during training; repeated experiments have found that setting it to 0.1 yields the best effect.

2.4. Precision Evaluation Index

In this paper, the coefficient of determination R^2 (R-squared), the root mean square error RMSE (root mean square error) and the mean absolute error MAE (mean absolute error) are used to evaluate the model fitting accuracy. R^2 is commonly used to measure the model's ability to account for variation, but is not suitable for comparing the performance of different models. RMSE and MAE, on the other hand, are more commonly used to evaluate the accuracy of predictive models, with RMSE being more sensitive to outliers and MAE providing an intuitive way to measure model error. The larger the R^2 value the better the model performance. the smaller the RMSE and MAE values the better the model performance. The formulas are shown below:

$$R^2 = 1 - \frac{\sum_{i=1}^n (y_i - \hat{y}_i)^2}{\sum_{i=1}^n (y_i - \bar{y})^2} \quad (7)$$

$$RMSE = \sqrt{\frac{1}{n} \sum_{i=1}^n (y_i - \hat{y}_i)^2} \quad (8)$$

$$MAE = \frac{1}{n} \sum_{i=1}^n |y_i - \hat{y}_i| \quad (9)$$

where y_i is the true value; \hat{y}_i is the predicted value; \bar{y} is the average of the true values.

3. Results

3.1. Model Accuracy Assessment

The model was validated on training and validation sets using R^2 , RMSE and MAE and compared with commonly used machine learning models in drought monitoring such as support vector machine (SVM) [35] and artificial neural network (ANN) [36] as well as the original unimproved LSTM model [37], as shown in Table 2. The results indicate that

the R^2 between the estimated CDMI values and the measured SPEI on the training set is 0.991 and on the validation set is 0.982; RMSEs are 0.094 and 0.141, and MAEs are 0.070 and 0.098, respectively, for the test and training sets. The model performs comparably on both the training and validation sets and shows significant improvements over the unimproved LSTM, SVM and ANN models. This demonstrates the high simulation accuracy of the AW-LSTM model, with good fitting and generalization capabilities on new data.

Table 2. Accuracy evaluation of AW-LSTM, LSTM, SVM and ANN models on validation and training sets.

Model	Train			Validation		
	R^2	RMSE	MAE	R^2	RMSE	MAE
AW-LSTM	0.991	0.094	0.070	0.982	0.141	0.098
LSTM	0.959	0.102	0.076	0.947	0.149	0.105
SVM	0.789	0.129	0.088	0.774	0.177	0.125
ANN	0.882	0.112	0.081	0.866	0.162	0.114

The AW-LSTM model demonstrates clear advantages over traditional machine learning models in drought monitoring for the following reasons: (1) The AW-LSTM enhances the LSTM's ability to process time-series data through the attention mechanism, enabling the model to focus on time points that have the greatest impact on the prediction outcome, thus improving accuracy. (2) The AW-LSTM model emphasizes key information in the time series by dynamically allocating weights, rather than treating all data points equally. This approach is particularly effective in capturing complex drought development patterns. (3) AW-LSTM uses regularization techniques and built-in gating mechanisms to prevent overfitting during model training, ensuring the model's generalization ability on unseen data.

Referring to the SPEI drought classification standard [38], CDMI values are categorized into extreme drought, severe drought, moderate drought, mild drought, normal, mildly moist, moderately moist, severely moist and extremely moist (Table 3). This paper calculated the concordance rate between the SPEI actual values and AW-LSTM model estimated values for drought grades, as shown in Table 4, where the concordance rate between actual SPEI values and training set estimated values (CDMI) is 89.2%, and between actual SPEI values and validation set estimated values (CDMI) is 87.8%. Additionally, we focused on analysing the spatiotemporal variations during the summer maize growing season (June–September) from 2018 to 2019, as shown in Figure 4, where (a) represents AW-LSTM model estimated values (CDMI) and (b) represents SPEI actual values. The analysis of this period can be considered a good estimate of the model's predictive ability for other periods. The diagram shows a high degree of consistency between model estimated values (CDMI) and SPEI actual values, with only minor differences in rare cases. For example, in September 2019, in southern Shandong Province, southern Henan Province and northern Huai North area, CDMI predicted severe drought while SPEI mostly indicated moderate drought, showing CDMI values were drier than SPEI values. Such local differences are common in predictions and are insufficient to affect the overall assessment and understanding of widespread drought trends. Overall, the model has high simulation accuracy and good predictive ability for new data, making it an effective tool for drought monitoring in the region, providing a favourable scientific basis for the prevention and mitigation of drought in the Huang-Huai-Hai Plain.

Table 3. Standardized Precipitation Evapotranspiration Index (SPEI) drought classification.

Level	Drought Type	SPEI Value
1	extremely moist	$SPEI \geq -2$
2	severely moist	$1.5 < SPEI < 2$
3	moderately moist	$1 < SPEI < 1.5$
4	mildly moist	$0.5 < SPEI < 1$
5	normal	$-0.5 < SPEI < 0.5$
6	mild drought	$-1 < SPEI \leq -0.5$
7	moderate drought	$-1.5 < SPEI \leq -1$
8	severe drought	$-2 < SPEI \leq -1.5$
9	extreme drought	$SPEI \leq -2$

Table 4. Analysis of consistency rates for AW-LSTM model predictions in training and validation sets.

Consistency Rate	
Training Set	89.2%
Validation Set	87.8%

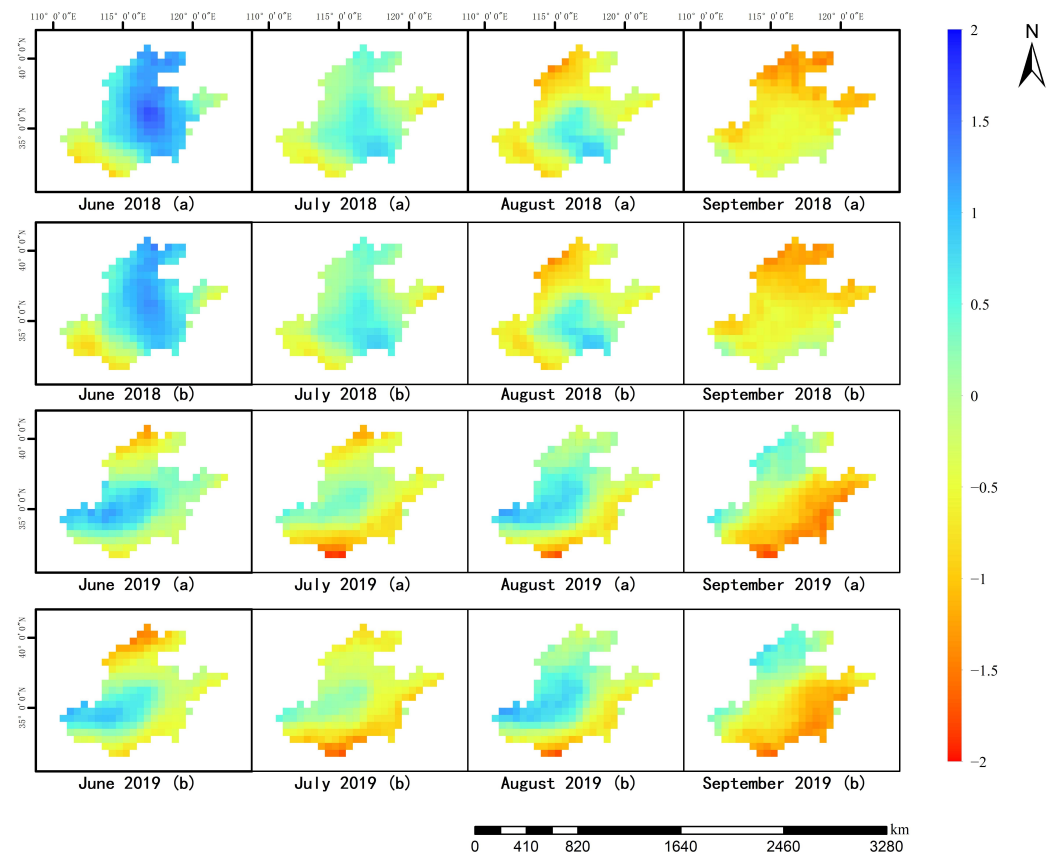


Figure 4. Drought monitoring during the summer maize growing season (June–September) from 2018 to 2019. (a) Model estimated values (CDMI). (b) SPEI actual values.

3.2. Correlation Analysis Based on Meteorological Drought

To validate the model’s capability in meteorological drought monitoring, this study used monthly temperature and precipitation data from 30 stations across the Huang-Huai-Hai Plain to calculate the Standardized Precipitation Evapotranspiration Index (SPEI) and conducted a validation analysis of the Composite Drought Monitoring Index (CDMI) estimated by the AW-LSTM model. SPEI integrates two key variables—precipitation

and temperature—not only sensitively reflecting changes in potential evaporation due to temperature changes but also the impact of precipitation amounts. SPEI has been widely used in global drought monitoring. Research shows that the SPEI-1, with a one-month timescale, is particularly suitable for monitoring meteorological drought because it can sensitively reflect short-term climatic changes and precipitation anomalies [39]. During the summer maize growing season from 2001 to 2022 (June to September), a correlation analysis between CDMI and SPEI-1 was conducted, with a scatter plot shown in Figure 5. The results indicate that CDMI has a strong correlation with SPEI-1, with all R^2 values above 0.85, except for June, which had an R^2 of 0.776, and all months passed the significance test with $p < 0.01$. This emphasizes the significant correlation between the CDMI constructed by the AW-LSTM model and the meteorological drought index during the summer maize growing season in the Huang-Huai-Hai Plain, demonstrating the model's excellent potential in meteorological drought monitoring.

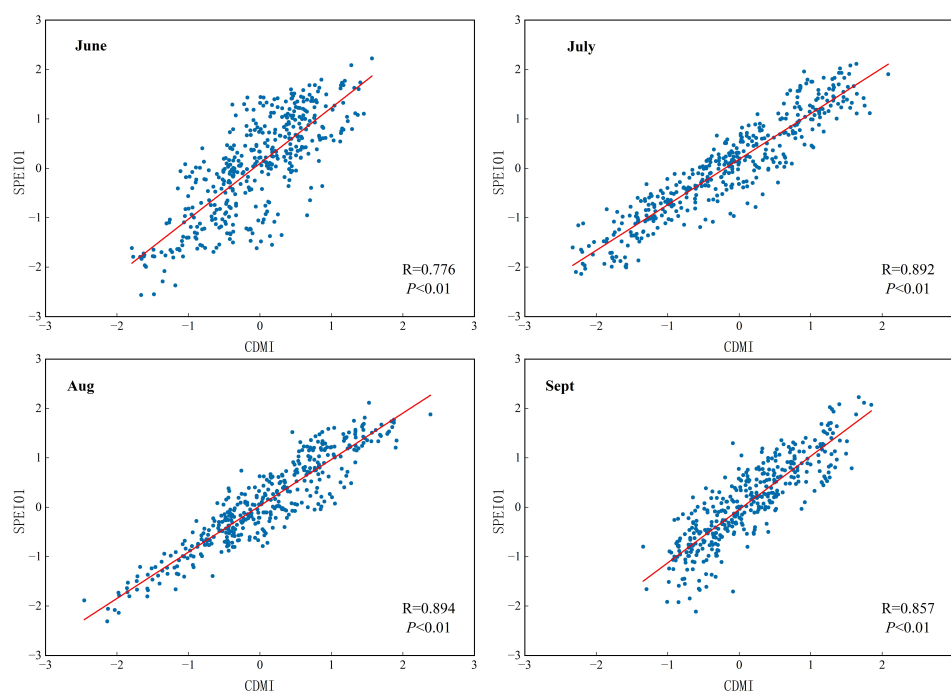


Figure 5. Scatter plot of CDMI versus SPEI with a one-month timescale.

3.3. Correlation Analysis Based on Agricultural Drought

To validate the model's applicability in agricultural drought monitoring, this study calculated the SPEI for a three-month timescale at 30 sites across the Huang-Huai-Hai Plain and conducted a validation analysis of the Composite Drought Monitoring Index (CDMI) estimated by the AW-LSTM model. The three-month SPEI is suitable for agricultural drought studies, focusing on soil moisture conditions and their impact on crop growth, which is typically related to longer periods of moisture accumulation and deficiency [39]. The three-month SPEI provides a comprehensive assessment of moisture conditions over time, better reflecting the average moisture conditions during the crop growing season. By calculating the SPEI-3 for the summer maize growing period (June–September) from 2001 to 2022, the correlation between SPEI-3 and the AW-LSTM model's estimated values (CDMI) was analysed, with a scatter plot of CDMI versus SPEI-3 shown in Figure 6. The results indicate that the correlation between CDMI and SPEI-3 is above 0.9, and both passed the significance test with $p < 0.01$, demonstrating the AW-LSTM model's excellent suitability in agricultural drought monitoring.

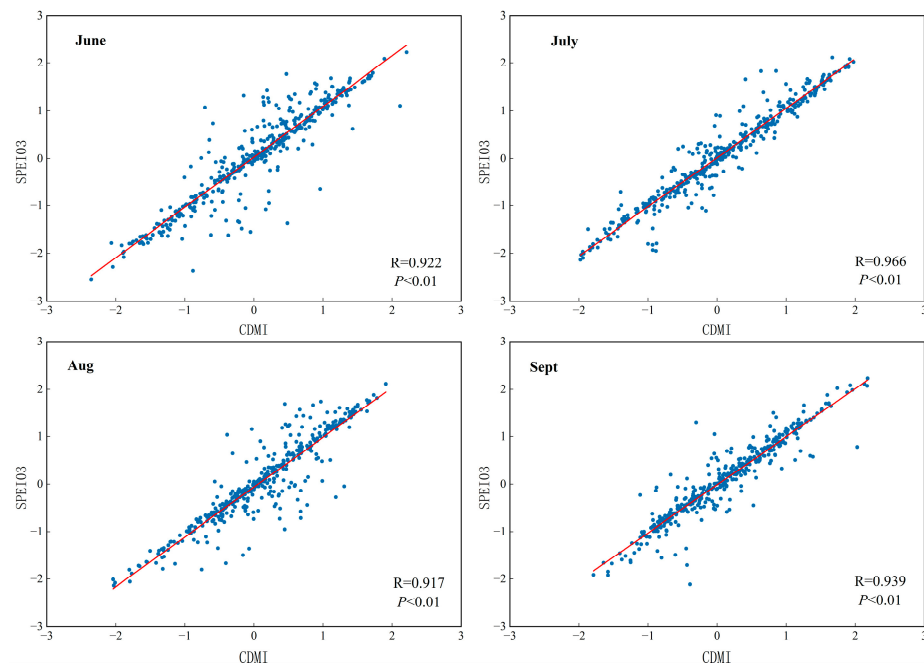


Figure 6. Scatter plot of CDMI versus SPEI with a three-month timescale.

Soil moisture is a decisive factor in agricultural drought [40]. To further validate the model's applicability in agricultural drought monitoring, this study analysed the correlation between 10 cm soil moisture and the Comprehensive Drought Monitoring Index (CDMI) at 30 sites during the summer maize growing season (June–September) from 2001 to 2022. The scatter plot of soil moisture and CDMI is shown in Figure 7. The results indicate that there is a strong correlation between CDMI and 10 cm soil moisture. The correlation coefficient in July is above 0.6, while in June, August and September, it exceeds 0.7, all passing the significance test with $p < 0.01$. The model-derived Comprehensive Drought Monitoring Index (CDMI) effectively reflects soil moisture information and can be applied to regional agricultural drought monitoring.

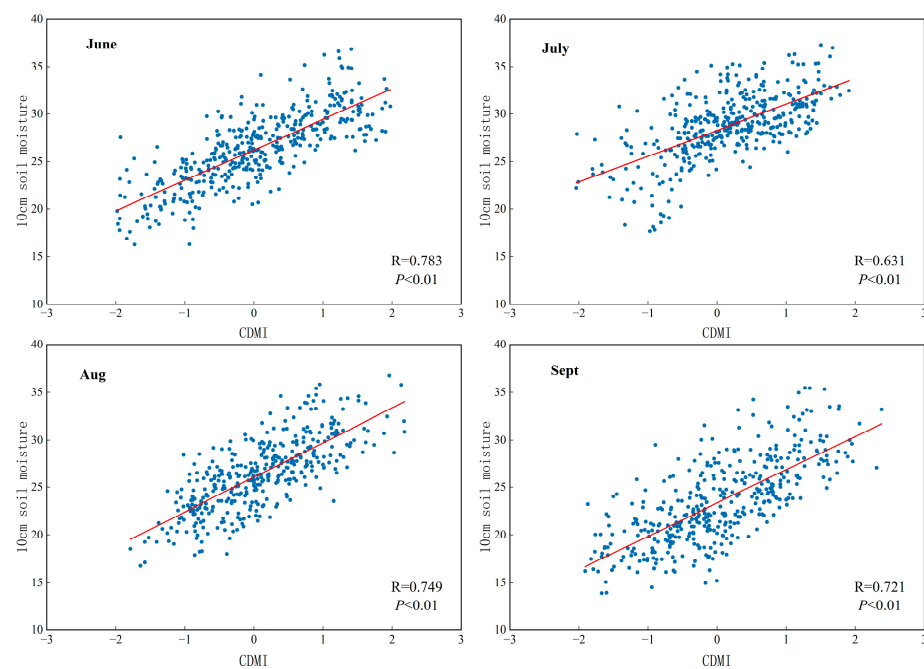


Figure 7. Scatter plot of CDMI versus 10 cm soil moisture.

In drought monitoring, it was found that the three-month SPEI (SPEI-3) performs better than the one-month SPEI (SPEI-1), and the validation results using soil moisture data are not as effective as those using SPEI. The main reason is that SPEI-3 covers a longer time frame, better reflecting the average or cumulative moisture conditions during the summer maize growing period in the Huang-Huai-Hai region. The three-month window aligns more closely with the sensitive period of crop growth water demands, making SPEI-3 more effective in agricultural drought monitoring. Soil moisture exhibits spatial heterogeneity at different locations, reducing the accuracy when applied across large areas; under drought conditions, human activities such as irrigation can impact soil moisture levels, thereby reducing the reliability of using soil moisture data for model validation.

3.4. Characteristics of the Spatial Distribution of the Huang-Huai-Hai Plain

3.4.1. Spatial Distribution Characteristics of the Huang-Huai-Hai Plain

The monthly CDMI data from 2001 to 2022 were compiled into an annual average CDMI and the compiled 22 annual average CDMI images were analysed using a linear trend (slope) method to assess the drought trends over 22 years in the Huang-Huai-Hai Plain. The slope trend map, shown in Figure 6, indicates that positive values represent an upward slope and negative values represent a downward slope. By calculating the slope of the drought index, the slope trend map clearly shows whether the severity of drought is increasing, decreasing or remaining stable. Positive coefficients indicate a decreasing trend in drought severity over time, while negative coefficients indicate an increasing trend. As shown in Figure 8, there is an increasing trend in drought severity in northern Hebei Province, Beijing, Tianjin, the southern Huai North area and central Henan Province. A decreasing trend is observed in the northern Huai North area, southern Shandong Province, western Henan Province and southwestern Hebei Province. The slope values in other areas are close to zero, indicating no significant change in drought conditions. This is consistent with the drought conditions described in the literature.

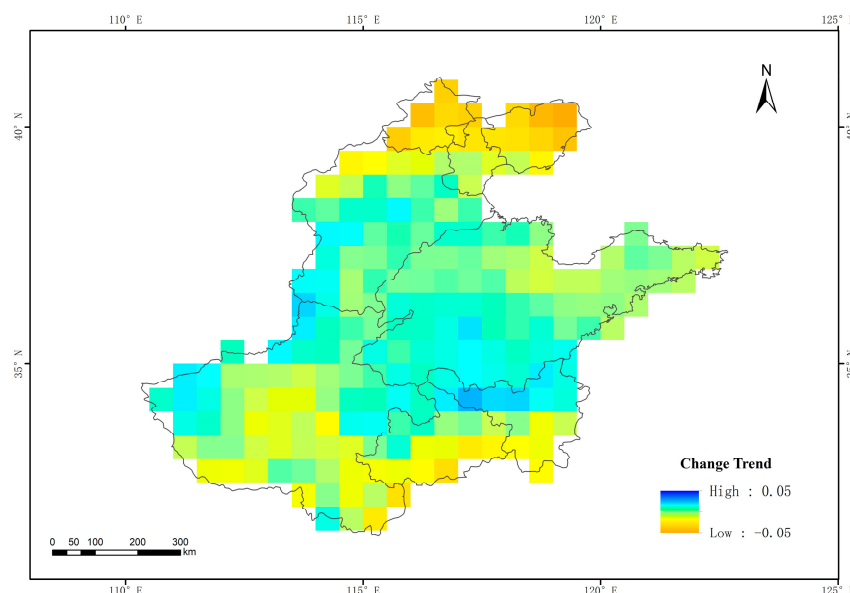


Figure 8. Huang-Huai-Hai Plain drought trends from 2001 to 2022.

For each summer maize growing season from 2001 to 2022 (June, July, August, September), 22 drought spatial distribution maps were synthesized, as shown in Figure 9. It is evident from the maps that agricultural drought in the Huang-Huai-Hai Plain is markedly regional and varies annually in extent and severity. In 2001, 2014, 2017 and 2019, droughts covered the entire Huang-Huai-Hai region. The droughts of 2014 and 2017 were primarily mild, whereas those of 2001 and 2019 were severe or predominantly moderate to severe. The severity of the drought decreased from the west to the east in 2001, from the northwest

to the southeast in 2014 and 2017 and from the northeast to the southwest in 2019. In 2002, 2006 and 2015, droughts primarily occurred in the northern parts of Hebei, Shandong and Henan provinces, with severity decreasing from northeast to southwest. In 2011, 2012, 2013 and 2022, droughts mainly affected the southern parts of Shandong and Henan provinces and the northern Huai region, with severity decreasing from southwest to northeast. In other years, droughts were mild, with the entire region primarily experiencing light or no drought conditions.

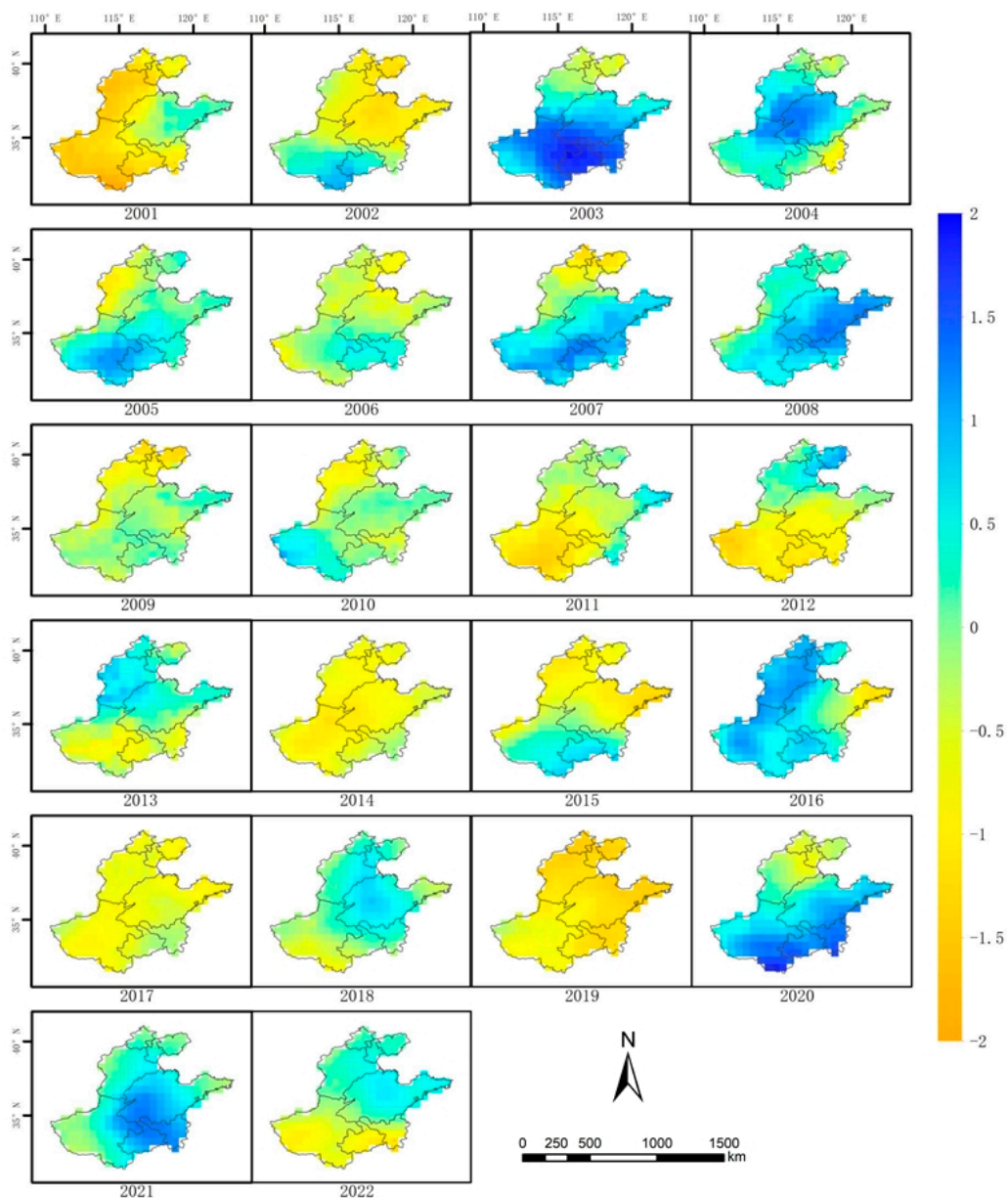


Figure 9. Spatial changes in the CDMI during the growing season in the Huang-Huai-Hai Plain from 2001 to 2022.

For the summer maize growing season in the Huang-Huai-Hai Plain, this study analysed the drought trend over 22 years from June to September of 2001 to 2022, using 22 images each month and applying the linear trend method (slope), as illustrated in Figure 10. Analysis of the figure shows that in June, the drought intensified in Beijing, Tianjin, Hebei, Shandong and the northeastern part of Henan, while other areas experienced a relief in drought trends. Similar trends of drought changes occurred in July, August and

September, with increased drought severity in the entire Henan Province and eastern Shandong, while drought in Beijing, Tianjin and northern Hebei eased.

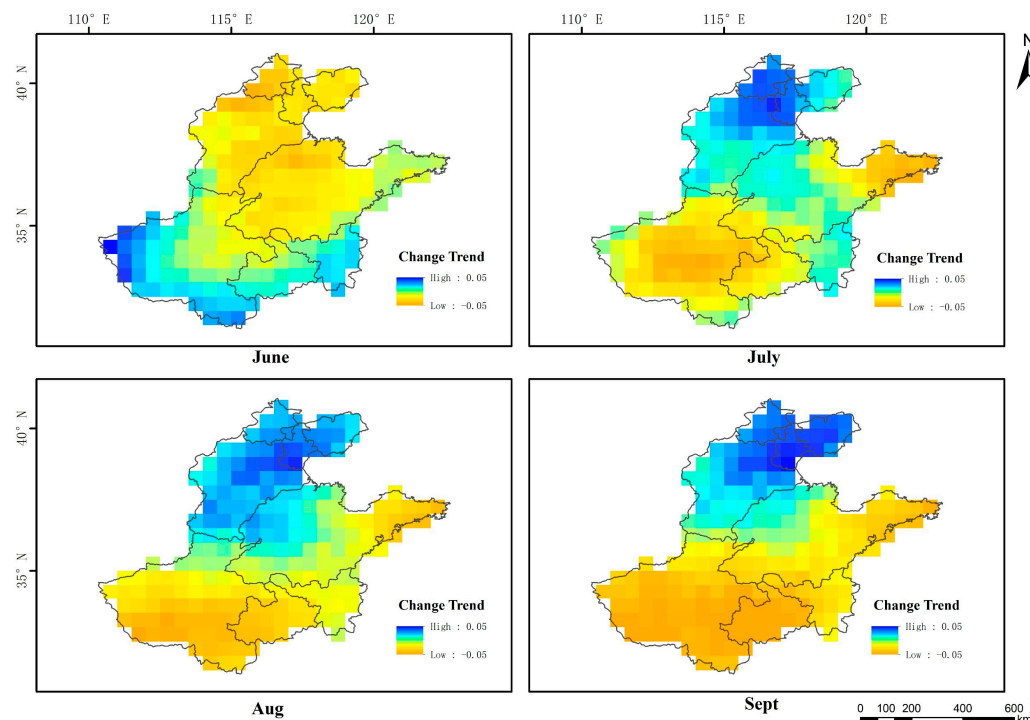


Figure 10. Drought spatial variation trends during the summer maize growing season (June–September) in the Huang-Huai-Hai Plain from 2001 to 2022.

3.4.2. Temporal Distribution Characteristics of the Huang-Huai-Hai Plain

Based on the AW-LSTM model, a comprehensive drought monitoring index (CDMI) was developed for 2001 to 2022. The monthly and annual average CDMI from June to September over these years was calculated, with monthly variations shown in Figure 11 and annual changes in Figure 12. The data shows that during 2001 to 2022, drought in the Huang-Huai-Hai Plain was variable, with significant droughts occurring in 2001, 2002, 2006, 2011, 2014 and 2019, particularly in 2001 and 2002, where most of the year experienced drought. This aligns with the three consecutive years of drought from 2000 to 2002, following the El Niño event of 1998. The CDMI showed fluctuations throughout the months, with more frequent droughts in June and September, while July and August were generally moister with fewer occurrences of drought. June marks the planting season for summer maize in the Huang-Huai-Hai Plain and September the harvest. During these critical agricultural phases, large areas of land are temporarily bare due to sowing and harvesting activities, reducing vegetation cover. This not only decreases the soil's ability to retain moisture but also increases evaporation, especially under the high temperatures of summer, exacerbating the onset and development of drought. Due to higher rainfall in July and August and the presence of major rivers like the Yellow, Huai and Hai rivers in the region, these factors collectively reduce the impact of drought. During these months, the ample rainfall and river water resources usually meet agricultural and other water demands, significantly mitigating the adverse effects of drought. Thus, drought does not greatly affect the region during this period.

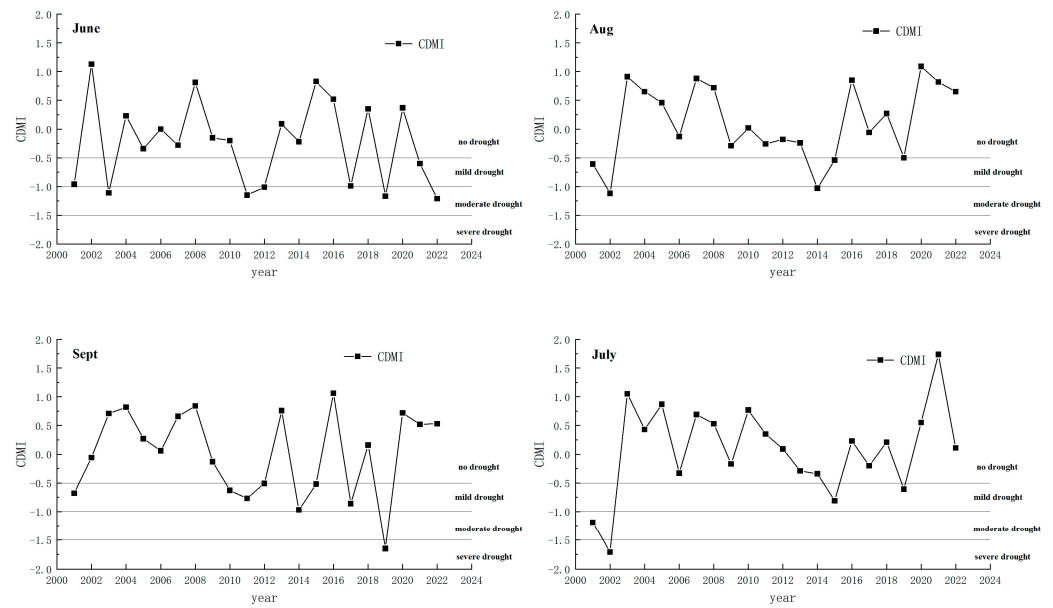


Figure 11. Monthly average changes in CDMI in the Huang-Huai-Hai Plain.

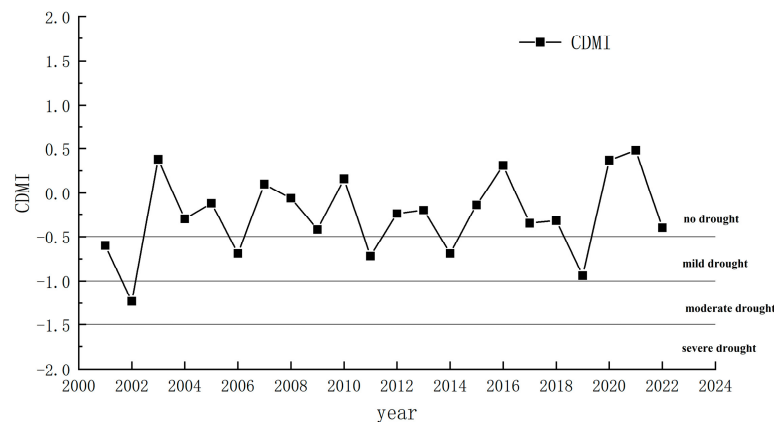


Figure 12. Annual average changes in CDMI in the Huang-Huai-Hai Plain.

4. Discussion

4.1. Impact of Land Cover Type

Land use classification maps for 2000 and 2021, as shown in Figure 2, categorize the land into five types: forests, grassland, water, urban and farmland. The analysis of the land cover proportions in the study area for these years reveals that the Huang-Huai-Hai Plain predominantly consists of farmland, urban land and forests. In 2000, farmland, urban and forests comprised 65.85%, 12.25% and 10.62% of the total area, respectively; in 2021, these figures changed to 54.91%, 22.55% and 3.84%. Other land cover types were minimal and can be disregarded in the study. From 2000 to 2021, the coverage of farmland and forests decreased by 10.94% and 6.87%, respectively, while urban areas increased by 10.3%. Moreover, the expansion of urban areas disrupted the water cycle, reduced rainfall and enhanced the urban heat island effect. This led to increased temperatures and evaporation, further exacerbating drought conditions. Forests have a significantly greater capacity to retain water than farmlands, especially in the western regions of Henan Province, where forest coverage is extensive. According to Figure 10, which shows the trends of change from June to September over 22 years, the reduction in drought was most significant in June. Despite an increase in drought severity in July, August and September, it remained below that of the surrounding areas.

4.2. The Impact of Different Factors on Drought

Additionally, this study analysed the impact of population, GDP, summer maize yield per unit area and agricultural water usage on drought. Table 5 provides statistics from 2006 to 2021 on population, GDP, summer maize yield per unit area and agricultural water usage. Figure 13 shows the trends over time for these variables. Additionally, average precipitation data from June to September from 2006 to 2021 were synthesized to calculate the average precipitation during the summer maize growing season, as shown in Figure 12. Analysis indicates that from 2006 to 2021, the population in the Huang-Huai-Hai Plain increased by 9.86%. The population growth led to increased food demand, which imposed higher demands on agricultural output, increasing the need for both land and water. The significant increase in GDP, coupled with rapid urban expansion, led to higher urban and industrial water usage, intensifying competition for water resources, not only reducing the water available for agriculture but also facing challenges due to the uneven distribution of rainfall. Figure 13 shows a decreasing trend in agricultural water supply, while summer maize, which has a high water demand, consumes significant amounts of agricultural water. The trends in precipitation over time, shown in Figure 14, are similar to those of the summer maize yield per unit area, indicating that precipitation remains the primary factor influencing drought under conditions of limited water resources. Considering the water resource challenges in the Huang-Huai-Hai Plain, especially in drought years, adopting reasonable and efficient water management strategies is crucial for ensuring summer maize yield. In summary, population growth and economic development in the Huang-Huai-Hai Plain not only increase the demand for summer maize but also provide opportunities to improve agricultural production conditions. Thus, drought monitoring and efficient water resource management are key to ensuring stable yields of summer maize, particularly when addressing climate risks such as drought.

Table 5. Population, GDP, summer corn yield per unit area and agricultural water usage, 2006–2021.

Time	Agricultural Water Usage (Billion Cubic Meters)	Corn Yield per Unit Sown Area (kg/ha)	Population (10,000 s)	GDP (Billion CNY)	Precipitation (mm)
2006	487.5	27,220.9	28,275	52,913.9	112.25
2007	456.9	27,903.1	28,461	64,279.4	147.18
2008	215.1	28,898.6	28,782	76,037.7	132.99
2009	576.0	28,325.7	29,079	82,639.2	115.31
2010	445.9	28,212.0	29,448	96,375.9	131.69
2011	436.7	29,810.4	29,723	112,069.6	122.35
2012	453.6	29,318.8	29,993	123,064.4	118.6
2013	450.5	29,539.1	30,142	134,316.4	114.32
2014	423.4	27,641.2	30,376	144,125.1	108.95
2015	417.4	28,679.1	30,539	154,429.9	109.76
2016	413.1	29,225.1	30,764	166,004.3	137.93
2017	388.7	30,425.0	30,848	180,811.4	120.57
2018	388.7	30,962.5	30,942	195,548.3	130.97
2019	387.2	31,489.0	31,029	208,737.5	109.01
2020	378.7	31,763.1	31,146	213,022.7	150.11

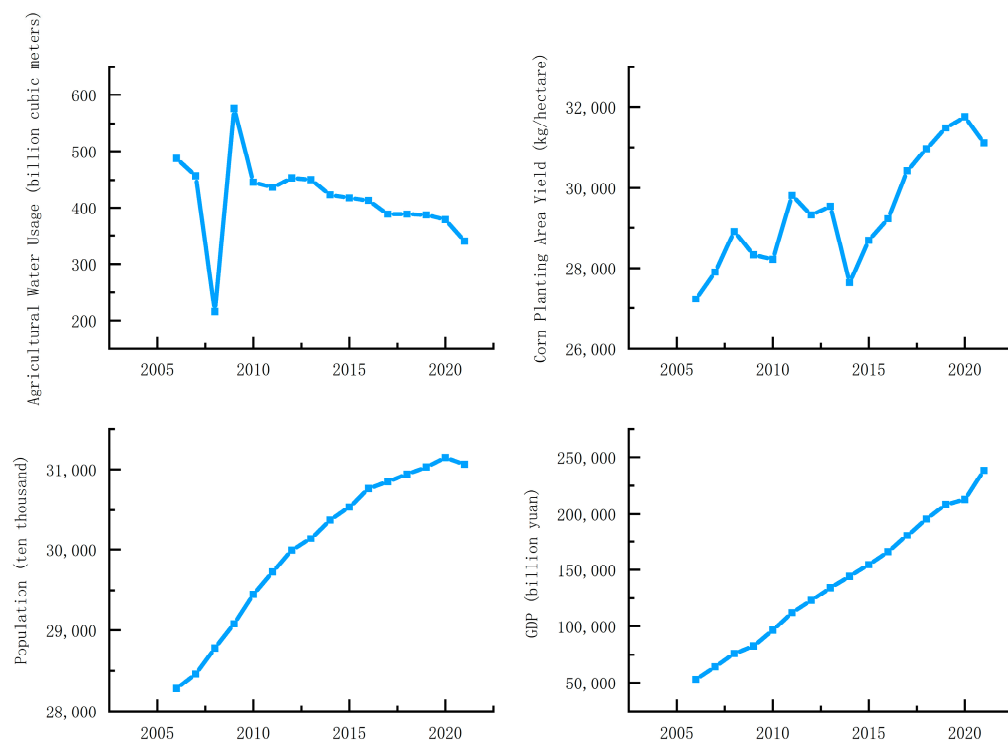


Figure 13. Trends in population, GDP, summer corn yield per unit area and agricultural water usage.

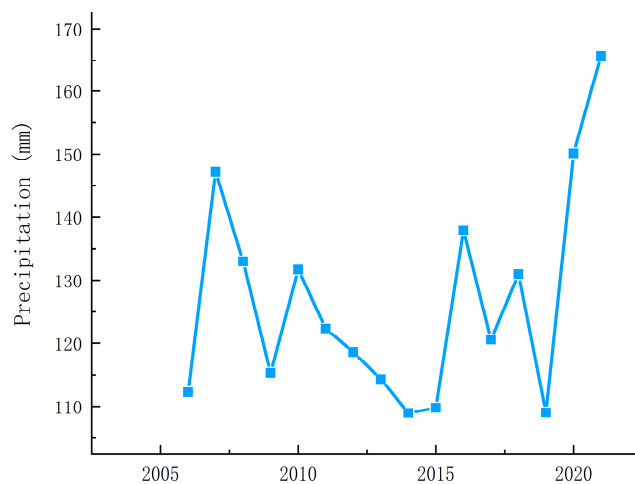


Figure 14. Changes in average precipitation during the summer corn growing season, 2006–2021.

4.3. Limitations of Drought Monitoring Models

The composite drought monitoring index CDMI, constructed using the AW-SLTM model in this study, has certain limitations that need to be further refined in future work. Here are the main constraints and directions for future development: (1) The spatial resolution of the CRU dataset used is too low. A single pixel contains different surface types, causing the calculation of drought indices to be affected by mixed pixel effects, which decreases accuracy. (2) Deep learning models have the capability to extract high-level features from a large number of low-level features. For this model, the more input factors, the more drought information it can unearth. In the future, it may be worth considering additional parameters such as soil moisture data and surface runoff data.

5. Conclusions

This study introduces an attention-weighted long short-term memory network model (AW-LSTM), which utilizes seven variables from the CRU dataset: precipitation, average temperature, cloud cover, vapor pressure, minimum/maximum temperature and potential evapotranspiration, to construct the Comprehensive Drought Monitoring Index (CDMI). The analysis of drought conditions in the Huang-Huai-Hai Plain from 2001 to 2022 led to the following conclusions:

- (1) The AW-LSTM model outperforms traditional LSTM, SVM and ANN models in drought monitoring, with a consistency rate of 89.2% on the training set and 87.8% on the validation set. The model is suitably applicable for both meteorological and agricultural drought monitoring. The correlation coefficient with the 1-month SPEI scale, excluding June, was above 0.85 ($p < 0.01$); for the 3-month SPEI scale, it exceeded 0.9 ($p < 0.01$) and it also showed good correlation with 10 cm soil moisture, exceeding 0.7 in all months except July ($p < 0.01$), demonstrating the AW-LSTM model's effectiveness in comprehensive agricultural drought monitoring.
- (2) Drought conditions in the Huang-Huai-Hai Plain show significant variability across different years and months. During the summer maize planting period, June and September are periods of relatively severe drought. In June, drought trends intensified in Shandong, Hebei, Beijing, Tianjin and northern Henan, while southern Henan and the Huai Bei area experienced drought relief; in July, August and September, as time progressed, drought trends intensified in Shandong, Henan and Huai Bei, but eased in Hebei, Beijing and Tianjin.
- (3) From 2001 to 2022, there has been a declining trend in cultivated land and forested areas, which has similarly contributed to the further occurrence of drought.

Author Contributions: Conceptualization, J.Z.; methodology, J.Z.; software, J.Z.; validation, J.Z.; formal analysis, J.Z.; investigation, J.Z.; resources, J.Z.; data curation, J.Z.; writing—original draft preparation, J.Z.; writing—review and editing, Y.F.; writing—review and editing, Q.G. and J.Z.; visualization, G.F.; supervision, Q.G.; project administration, Y.F.; funding acquisition, Y.F. All authors have read and agreed to the published version of the manuscript.

Funding: This research was funded by the National Natural Science Youth Fund (42106215), Shandong Natural Science Youth Fund (ZR202103030691), Self-innovation Project-Strategic Special Project (22CX01004A-3) and Science and Technology Unveiling Special Project (2201-34).

Data Availability Statement: The original contributions presented in the study are included in the article, further inquiries can be directed to the corresponding author.

Conflicts of Interest: The authors declare no conflicts of interest. The funders had no role in the design of the study; in the collection, analyses, or interpretation of data; in the writing of the manuscript; or in the decision to publish the results.

References

1. Singh, W.R.; Barman, S.; Vijayakumar, S.V.; Hazarika, N.; Kalita, B.; Taggu, A. Drought Assessment in the Districts of Assam Using Standardized Precipitation Index. *J. Earth Syst. Sci.* **2024**, *133*, 43. [\[CrossRef\]](#)
2. Khan, N.; Shahid, S.; Chung, E.-S.; Kim, S.; Ali, R. Influence of Surface Water Bodies on the Land Surface Temperature of Bangladesh. *Sustainability* **2019**, *11*, 6754. [\[CrossRef\]](#)
3. Ezzine, H.; Bouziane, A.; Ouazar, D. Seasonal Comparisons of Meteorological and Agricultural Drought Indices in Morocco Using Open Short Time-Series Data. *Int. J. Appl. Earth Obs. Geoinf.* **2014**, *26*, 36–48. [\[CrossRef\]](#)
4. Wang, Y.; Zhang, Q.; Wang, J.; Han, L.; Wang, S.; Zhang, L.; Yao, Y.; Hao, X.; Wang, S. New progress and prospect of drought research since the 21st century. *J. Arid Meteorol.* **2022**, *40*, 549–566.
5. Zhang, Q.; Yao, Y.; Li, Y.; Huang, J.; Ma, Z.; Wang, Z.; Wang, S.; Wang, Y.; Zhang, Y. Progress and prospect on the study of causes and variation regularity of droughts in China. *Acta Meteorol. Sin.* **2020**, *78*, 500–521. [\[CrossRef\]](#)
6. Zhang, J.; Qu, Y. Exploration of Drought Disaster Evolution Patterns and Drought Relief Strategies in China Over the Past 30 Years. *China Flood Drought Manag.* **2008**, *18*, 47–52. [\[CrossRef\]](#)
7. Compilation Group of China Flood and Drought Disaster Prevention Bulletin. Summary of China Flood and Drought Disaster Prevention Bulletin 2022. *China Flood Drought Manag.* **2023**, *33*, 78–82. [\[CrossRef\]](#)

8. Baniya, B.; Tang, Q.; Xu, X.; Haile, G.; Chhipi-Shrestha, G. Spatial and Temporal Variation of Drought Based on Satellite Derived Vegetation Condition Index in Nepal from 1982–2015. *Sensors* **2019**, *19*, 430. [[CrossRef](#)] [[PubMed](#)]
9. Liu, C.; Yang, C.; Yang, Q.; Wang, J. Spatiotemporal Drought Analysis by the Standardized Precipitation Index (SPI) and Standardized Precipitation Evapotranspiration Index (SPEI) in Sichuan Province, China. *Sci. Rep.* **2021**, *11*, 1280. [[CrossRef](#)]
10. Deng, H.; Cheng, F.; Wang, J.; Wang, C. Monitoring of Drought in Central Yunnan, China Based on TVDI Model. *Pol. J. Environ. Stud.* **2021**, *30*, 3511–3523. [[CrossRef](#)]
11. Jiao, W.; Wang, L.; Novick, K.A.; Chang, Q. A New Station-Enabled Multi-Sensor Integrated Index for Drought Monitoring. *J. Hydrol.* **2019**, *574*, 169–180. [[CrossRef](#)]
12. Zhang, Q.; Shi, R.; Xu, C.-Y.; Sun, P.; Yu, H.; Zhao, J. Multisource Data-Based Integrated Drought Monitoring Index: Model Development and Application. *J. Hydrol.* **2022**, *615*, 128644. [[CrossRef](#)]
13. Saha, S.; Gogoi, P.; Gayen, A.; Paul, G.C. Constructing the Machine Learning Techniques Based Spatial Drought Vulnerability Index in Karnataka State of India. *J. Clean. Prod.* **2021**, *314*, 128073. [[CrossRef](#)]
14. Proadhan, F.A.; Zhang, J.; Yao, F.; Shi, L.; Pangali Sharma, T.P.; Zhang, D.; Cao, D.; Zheng, M.; Ahmed, N.; Mohana, H.P. Deep Learning for Monitoring Agricultural Drought in South Asia Using Remote Sensing Data. *Remote Sens.* **2021**, *13*, 1715. [[CrossRef](#)]
15. Wang, S.; Mo, X.; Hu, S.; Liu, S.; Liu, Z. Assessment of Droughts and Wheat Yield Loss on the North China Plain with an Aggregate Drought Index (ADI) Approach. *Ecol. Indic.* **2018**, *87*, 107–116. [[CrossRef](#)]
16. Yu, H.; Li, L.; Li, J. Establishment of comprehensive drought monitoring model based on downscaling TRMM and MODIS data. *J. Nat. Resour.* **2020**, *35*, 2553. [[CrossRef](#)]
17. Xu, L.; Chen, N.; Yang, C.; Zhang, C.; Yu, H. A Parametric Multivariate Drought Index for Drought Monitoring and Assessment under Climate Change. *Agric. For. Meteorol.* **2021**, *310*, 108657. [[CrossRef](#)]
18. Arun Kumar, K.C.; Reddy, G.P.O.; Masilamani, P.; Turkar, S.Y.; Sandeep, P. Integrated Drought Monitoring Index: A Tool to Monitor Agricultural Drought by Using Time-Series Datasets of Space-Based Earth Observation Satellites. *Adv. Space Res.* **2021**, *67*, 298–315. [[CrossRef](#)]
19. Sundararajan, K.; Garg, L.; Srinivasan, K.; Kashif Bashir, A.; Kaliappan, J.; Pattukandan Ganapathy, G.; Kumaran Selvaraj, S.; Meena, T. A Contemporary Review on Drought Modeling Using Machine Learning Approaches. *Comput. Model. Eng. Sci.* **2021**, *128*, 447–487. [[CrossRef](#)]
20. Proadhan, F.A.; Zhang, J.; Hasan, S.S.; Pangali Sharma, T.P.; Mohana, H.P. A Review of Machine Learning Methods for Drought Hazard Monitoring and Forecasting: Current Research Trends, Challenges, and Future Research Directions. *Environ. Model. Softw.* **2022**, *149*, 105327. [[CrossRef](#)]
21. Janiesch, C.; Zschech, P.; Heinrich, K. Machine Learning and Deep Learning. *Electron Mark.* **2021**, *31*, 685–695. [[CrossRef](#)]
22. Huang, Y. Research on Remote Sensing Derived Agricultural Drought Monitoring Method and Its Adaptability Evaluation Concerning Spatiotemporal Multi-Factor. Ph.D. Thesis, China University of Geosciences, Wuhan, China, 2021. [[CrossRef](#)]
23. Dikshit, A.; Pradhan, B.; Huete, A. An Improved SPEI Drought Forecasting Approach Using the Long Short-Term Memory Neural Network. *J. Environ. Manag.* **2021**, *283*, 111979. [[CrossRef](#)] [[PubMed](#)]
24. Yuan, Z.; Yan, D.-H.; Yang, Z.-Y.; Yin, J.; Yuan, Y. Temporal and Spatial Variability of Drought in Huang-Huai-Hai River Basin, China. *Theor. Appl. Clim.* **2015**, *122*, 755–769. [[CrossRef](#)]
25. Huang, Q.; Wang, L.; Chen, Z.; Liu, H. Effects of Meteorological Factors on Different Grades of Winter Wheat Growth in the Huang-Huai-Hai Plain, China. *J. Integr. Agric.* **2016**, *15*, 2647–2657. [[CrossRef](#)]
26. Shi, X.; Ding, H.; Wu, M.; Zhang, N.; Shi, M.; Chen, F.; Li, Y. Effects of Different Types of Drought on Vegetation in Huang-Huai-Hai River Basin, China. *Ecol. Indic.* **2022**, *144*, 109428. [[CrossRef](#)]
27. *National Report on the Quality Grades of Cultivated Land 2019*; Agricultural Comprehensive Development in China: Beijing, China, 2020; pp. 6–12.
28. Xue, C.; Liu, R.; Ma, Z. Drought grade classification of summer maize in Huang-Huai-Hai area. *Trans. Chin. Soc. Agric. Eng. (Trans. CSAE)* **2014**, *30*, 147–156. [[CrossRef](#)]
29. Sun, Q.; Miao, C.; Duan, Q.; Ashouri, H.; Sorooshian, S.; Hsu, K. A Review of Global Precipitation Data Sets: Data Sources, Estimation, and Intercomparisons. *Rev. Geophys.* **2018**, *56*, 79–107. [[CrossRef](#)]
30. Spinoni, J.; Barbosa, P.; De Jager, A.; McCormick, N.; Naumann, G.; Vogt, J.V.; Magni, D.; Masante, D.; Mazzeschi, M. A New Global Database of Meteorological Drought Events from 1951 to 2016. *J. Hydrol. Reg. Stud.* **2019**, *22*, 100593. [[CrossRef](#)] [[PubMed](#)]
31. Bengio, Y.; Frasconi, P.; Simard, P. The Problem of Learning Long-Term Dependencies in Recurrent Networks. In Proceedings of the IEEE International Conference on Neural Networks, San Francisco, CA, USA, 28 March–1 April 1993; IEEE: San Francisco, CA, USA, 1993; pp. 1183–1188.
32. Hochreiter, S.; Schmidhuber, J. Long Short-Term Memory. *Neural Comput.* **1997**, *9*, 1735–1780. [[CrossRef](#)]
33. Botvinick, M.M.; Plaut, D.C. Short-Term Memory for Serial Order: A Recurrent Neural Network Model. *Psychol. Rev.* **2006**, *113*, 201–233. [[CrossRef](#)]
34. Tian, C.; Ma, J.; Zhang, C.; Zhan, P. A Deep Neural Network Model for Short-Term Load Forecast Based on Long Short-Term Memory Network and Convolutional Neural Network. *Energies* **2018**, *11*, 3493. [[CrossRef](#)]
35. Khan, N.; Sachindra, D.A.; Shahid, S.; Ahmed, K.; Shiru, M.S.; Nawaz, N. Prediction of Droughts over Pakistan Using Machine Learning Algorithms. *Adv. Water Resour.* **2020**, *139*, 103562. [[CrossRef](#)]

36. Vidyarthi, V.K.; Jain, A. Knowledge Extraction from Trained ANN Drought Classification Model. *J. Hydrol.* **2020**, *585*, 124804. [[CrossRef](#)]
37. Dikshit, A.; Pradhan, B.; Alamri, A.M. Long Lead Time Drought Forecasting Using Lagged Climate Variables and a Stacked Long Short-Term Memory Model. *Sci. Total Environ.* **2021**, *755*, 142638. [[CrossRef](#)] [[PubMed](#)]
38. Vicente-Serrano, S.M.; Beguería, S.; López-Moreno, J.I. A Multiscalar Drought Index Sensitive to Global Warming: The Standardized Precipitation Evapotranspiration Index. *J. Clim.* **2010**, *23*, 1696–1718. [[CrossRef](#)]
39. Wang, Q.; Shi, P.; Lei, T.; Geng, G.; Liu, J.; Mo, X.; Li, X.; Zhou, H.; Wu, J. The Alleviating Trend of Drought in the Huang-Huai-Hai Plain of China Based on the Daily SPEI. *Int. J. Climatol.* **2015**, *35*, 3760–3769. [[CrossRef](#)]
40. Shen, R.; Huang, A.; Li, B.; Guo, J. Construction of a Drought Monitoring Model Using Deep Learning Based on Multi-Source Remote Sensing Data. *Int. J. Appl. Earth Obs. Geoinf.* **2019**, *79*, 48–57. [[CrossRef](#)]

Disclaimer/Publisher’s Note: The statements, opinions and data contained in all publications are solely those of the individual author(s) and contributor(s) and not of MDPI and/or the editor(s). MDPI and/or the editor(s) disclaim responsibility for any injury to people or property resulting from any ideas, methods, instructions or products referred to in the content.